Egyptian Journal of Radiology and Nuclear Medicine

RESEARCH Open Access

Whole body diffusion-weighted MRI in detection of metastasis and lymphoma: a prospective longitudinal clinical study

Heba H. Goda[1*], Abd Elkareem H. AbdAllah[1], Eman A. Ahmed[1], Hassan I. Megally[1], Marwa I. Khalaf[2], Ahmed M. Taha[3] and Hosam Eldeen G. Mohamed[1]

Abstract

Background: Whole-body diffusion-weighted magnetic resonance imaging (WB-DWI-MRI) is an emerging tool that has an increasing role in the diagnosis of metastasis and lymphoma. This is a longitudinal study in actual clinical settings designed to assess WB-DWI-MRI in detection of tumor spread. The study included all patients who were referred to Radiology Department, during the period from June 2016 till May 2018, with either a known primary tumor (either laboratory, radiologically, or histologically proven, of any type, affecting any organ) or with biopsy-proven lymphoma of any subtype, affecting any organ. All patients underwent WB coronal T1-weighted, STIR, axial T2-weighted, and DWI-MRI examinations before commencing any treatment with curative intent. The body was divided into lymph nodes (LNs), skeletal system, and organs (brain, lung, and liver). Patients were followed up till the nature of the lesion(s) was confirmed (clinically, radiologically, or histologically).

Results: The study included 46 patients; 27 patients had metastases and 19 had lymphomas. Sensitivities, specificities, and accuracies for LN detection were 77%, 85%, and 83%; for skeletal metastasis were 88%, 94%, and 92%; for brain lesions were 78%, 95%, and 91%; and for lung lesion were 64%, 88%, and 76%, respectively. As for the liver, all lesions were correctly identified and did not miss any lesion with accuracy of 100%. Overall, 1739 lesions were discovered in 1271 regions out of 3818 examined regions with overall sensitivity, specificity, and accuracy of 86%, 92%, and 90% respectively.

Conclusion: The diagnostic performance of WB-DWI-MRI is variable among different anatomical sites. It has good performance in diagnosis of some organs as liver, bone marrow, and some LNs regions as porta-hepatis. It has a less diagnostic performance in the lung, and LNs located in cervical, mediastinum, supraclavicular, and mesenteric regions.

Keywords: WB-MR imaging, DWI, Metastasis, Lymphoma, Neoplasm

Background

Metastatic lesions are common manifestations of advanced cancers with very high prevalence in current practice. It is becoming an everyday clinical question [1]. Malignant lymphoma is another relatively common tumor that requires accurate staging at initial presentation that is essential for treatment planning and prognostication. Clinicians are highly dependent upon different imaging procedures for staging that takes into account the number of involved sites and the type of lesions (nodal or extra-nodal) [2].

Whole-body diffusion-weighted magnetic resonance imaging (WB-DWI-MRI) is an emerging tool that has been developed to assess tumor spread. Combining MRI's unique power of characterizing tissues, based on water and fat content, with DWI's ability to assess tissue water motion, provides a unique tool to both detect and

* Correspondence: hebagoda08@googlemail.com
[1]Radiology Department, Faculty of Medicine, Assiut University, Assiut, Egypt
Full list of author information is available at the end of the article

characterize lesions within tissues. Positron emission/computed tomography (PET/CT) is considered the preferred investigation in secondaries detection in clinical guidelines [3]. WB-DWI-MRI is probably the closest competitor to PET/CT scanning. As PET/CT, it covers the whole body and gives exquisite anatomical identification as it is always done in association with other MRI sequences and has the capability to be considered "functional" scanning. But unlike PET/CT, it avoids ionizing radiation, of lower cost, and does not require radioactive tracers. Also, PET/CT has low sensitivity in detecting metastasis in the brain and liver, due to the high physiological tracer uptake in these organs [3].

In this study, we tried to explore the value of WB-DWI-MRI in detecting metastases, in clinical settings, by including different types of malignancies and lymphomas in a single study.

Methods

The study was prospective. Written informed consents were obtained from all patients for their data to be included in the study. Institutional ethical committee approval was obtained. The study included all patients referred to Radiology Department, during the period from June 2016 till May 2018, with a known primary or lymphoma, that were laboratory, radiologically, or histologically proven, of any type, affecting any organ. All patients underwent WB-DWI-MRI before commencing any treatment of the primary lesion (surgery, radiotherapy or chemotherapy). All included patients had no contraindication for MRI examination. The study excluded patients in whom a confirmatory method of the nature of the possibly metastatic lesion was not available. Patients who did not show any metastatic lesion in the scans were also excluded.

Confirmation of the nature of the lesion

The identified lesion(s) was considered a metastasis if it was confirmed histologically by a diagnostic biopsy that was done for clinical needs. Alternatively, if this was not available, clinical and radiological progress were followed till identification of the true nature of the lesion. All radiological investigations done during the follow-up period were requested for the clinical needs of patients, and at the discretion of the responsible physician.

MRI technique

All patients had MRI according to the study protocol. The machine used was Gyroscan Philips 1.5 Tesla strength ACS-NT synergy coil, Holland. No contrast media was used. The patients lied supine on MRI table with hands beside his body. Conventional techniques used were coronal T1-weighted images (WI), coronal STIR, axial T2-WI images, and sagittal STIR of the spine. Then, WB-DWI-MRI was obtained. Parameters are summarized in Table 1. Images were acquired with a built-in body coil for signal reception, from head to toes, under free breathing. The total acquisition time for WB-conventional and DWI-MRI was approximately 40–45 min including 20–25 min for WB-DWI. Axial images were reconstructed on a coronal plane; then the reconstructed images in the coronal plane for each station were merged to obtain a coronal WB images. Color-coded fused T1-DWI images and apparent diffusion coefficient (ADC) maps were generated by Phillips workstation software.

Image interpretation

The images for MRI were prospectively assessed for each patient by two radiologists who have more than 5 years' experience in MRI imaging. For the purpose of the research, the body was divided into three groups: lymph nodes (LNs), skeletal system, and organs. Then, LN groups were further divided into 16 regions and skeletal system was divided into 63 regions. Organs considered in the study are the three organs commonly involved which are the brain, lungs, and liver, and a fourth group that includes the other organs. Criteria for involvement were either local or diffuse hypo intensities in T1-WI or hyper intensities in T2-WI and STIR images or restricted diffusion in DWI or hypo-intensity on ADC maps or their combinations. Post-processing ADC values and maps were done separately for each anatomical location through the workstation software. Lowest ADC values were measured using a region of interest in the center of the lesion avoiding necrotic and cystic areas. A cut-off value of 1×10^{-3} mm^2/s was used to differentiate restricted areas from non-restricted areas. A LN was considered positive if its short diameter was equal to or more than 10 mm, loss of fatty hilum, irregular margins or apparent speculation, diffusion restriction, and low ADC value where a cut-off value of 0.8×10^{-3} mm^2/s was used.

Statistical analysis

Analysis will be performed using SPSS 18.0 software (SPSS Chicago, IL, USA). The sensitivity, specificity, accuracy, positive predictive value, and negative predictive value were calculated and expressed per region not per patient.

Results

This study included 46 patients; (25 males and 21 females, median age was 49, range 16 to 79 years); 27 patients had metastases of a known primary tumor and 19 had lymphomas. Distribution according to primary site is shown in Table 2.

Table 1 Parameters of WB-MRI technique

	T1W	T2W	STIR	DWI (*b* value 0,1000)
TR; ms	537	1179	6564 Inversion time 130	6960 Inversion time 150
TE; ms	20	80	70	79
Reconstruction matrix	512 × 512	512 × 512	512 × 512	512 × 512
Slice thickness; mm	7	7	7	7

Methods of confirmation of the nature of the lesions

Radiological follow-up by different imaging techniques was the method of confirmation of the nature of the lesion in most of the occasions. Follow-up ranged from 6 to 12 months. Table 3 shows the number of scans done in patients in this study that were used for confirmation. Most patients had underdone more than one imaging modality during follow-up. Only 4 lesions had been biopsied; 2 from liver, 1from lung, and 1 from a neck LN.

Diagnostic performance of WB-MRI

Results are shown in Tables 4 and 5. Regarding LN detection, WB-DWI-MRI detected 233 out of all 736 possible LN regions in all patients. Sensitivity, specificity, and accuracy for LN detection were 77%, 85%, and 83%, respectively. WB-DWI-MRI showed highest sensitivity in femoral groups of LNs followed by inguinal and porta-hepatis groups of LN's. On the other hand, it was the lowest in the supraclavicular and mediastinal groups of LNs. The highest false-positive results were in axillary and inguinal LNs, while the mediastinal, supraclavicular, and cervical LNs showed the highest false-negative results (Fig. 1).

For skeletal metastasis, WB-DWI-MRI detected lesions in 984 out of 2898 regions in all patients. Sensitivity, specificity, and accuracy were 88%, 94%, and 92%, respectively. In all regions, sensitivity ranged between 80 and 92% except for pubic bones where it was 60% (Fig. 2).

Table 2 Distribution according to primary site

Organ	Frequency
Breast	8
Prostate	5
Liver	4
Colon	3
Thyroid	2
Lung	2
Ovaries	2
Testes	1
HL	11
NHL	8
Total	46

Abbreviations: *HL* Hodgkin's lymphoma, *NHL* non-Hodgkin's lymphoma

For brain lesions, sensitivity, specificity, and accuracy were 78%, 95%, and 91%, respectively. In 46 patients, 9 patients had 13 brain lesions; of them, 2 were false-positive and 2 were false-negative. For lung lesions, sensitivity, specificity, and accuracy were 64%, 88%, and 76% respectively. Fifty-four lesions were identified in 17 patients; of them, 3 were false-positive and 8 were false-negative (Fig. 3 and 4). As regards the liver, WB-DWI-MRI detected correctly all 52 lesions in 16 patients and did not miss any lesion with accuracy of 100% in this study (Fig. 5).

Overall, 1739 lesions were discovered by WB-DWI-MRI in 1271 regions out of 3818 examined regions; 1069 regions were true-positive and 176 regions were missed and were later proved to be malignant, whereas 202 regions were false-positive. Overall sensitivity, specificity, and accuracy were 86%, 92%, and 90%, respectively.

Discussion

This research was intended to be an exploratory research of the applicability of WB-DWI-MRI. It was a prospective clinical study, in which the patients were followed up till a clarification of the nature of the lesion had been reached. So, the researchers are naturally blind to the actual nature of the lesion. In most similar studies, comparisons are made with other concurrently done scans that have their own inherent accuracies. Additionally, for this study to be as beneficial and reproducible as possible, we tried to simulate the actual clinical scenario that the radiographer is exposed to in his/her daily activities. So, we combined the data from the conventional MRI to that of DWI-MRI and did not try to compare

Table 3 Scans done for confirmation of the nature of the lesions

Mode of confirmation	Number of patients
CT Chest	31
Ultrasound abdomen and pelvis	31
CT/MRI abdomen and pelvis	29
Bone scan	22
Ultrasound neck	13
PET/CT	12
Ultrasound/mammography/MRI breast	8
Biopsy	4
MRI FLAIR for brain lesions	2

Table 4 Number of regions involved and lesions detected by WB-MRI, distributed per patient pathology

		Breast (no = 8)		Prostate (no = 5)		Liver (no = 4)		Colon (no = 3)		Thyroid (no = 2)		Lungs (no = 2)		Ovaries (no = 2)		Testes (no = 1)		HL (no = 11)		NHL (no = 8)		Total (no = 46)	
		R	L	R	L	R	L	R	L	R	L	R	L	R	L	R	L	R	L	R	L	R	L
LNs (16 regions)	2 × cervical	6	13	5	7	2	4	0	0	1	3	1	4	0	0	0	0	14	20	10	12	39	63
	Mediastinal	3	6	1	2	0	0	0	0	1	4	2	6	0	0	0	0	6	10	2	6	15	34
	2 × supra-clavicular	5	11	1	3	0	0	0	0	2	4	1	3	0	0	0	0	4	8	2	6	15	35
	2 × axillary	12	24	5	5	3	5	4	6	1	3	1	3	1	2	0	0	10	15	8	20	45	83
	Para-aortic	1	3	3	5	1	2	1	3	0	0	0	0	2	8	1	4	6	13	2	8	17	46
	Porta-hepatis	0	0	0	0	3	6	3	5	0	0	0	0	0	0	0	0	2	4	1	2	9	17
	Mesenteric	0	0	0	0	2	5	3	9	0	0	0	0	0	0	0	0	4	8	2	8	11	30
	2 × iliac	2	4	4	5	2	4	0	0	0	0	0	0	2	6	1	2	9	11	4	8	24	40
	2 × femoral	1	2	2	2	2	5	0	0	1	2	1	2	1	4	1	2	8	14	4	10	21	43
	2 × inguinal	9	18	6	9	5	7	0	0	1	4	1	2	2	8	1	3	6	12	6	11	37	74
	Total LNs	39	81	27	38	20	38	11	23	7	20	7	20	8	28	4	11	69	115	41	91	233	465
Skeletal system (63 regions)	Skull	4	5	2	3	0	0	0	0	1	2	1	3	0	0	0	0	2	3	2	4	12	20
	2 × clavicle	10	11	5	5	4	4	0	0	2	3	0	0	1	1	0	0	4	8	8	10	34	42
	Sternum	5	5	2	2	2	2	0	0	2	2	0	0	0	0	0	0	2	3	4	6	17	20
	2 × humerus	12	18	6	8	4	6	2	4	1	3	0	0	1	3	1	2	6	8	6	12	39	64
	24 × ribs	70	72	56	57	18	19	10	10	10	10	12	12	0	0	0	0	96	101	86	86	358	367
	7 × cervical vertebrae	10	10	13	13	6	6	0	0	4	4	4	4	4	4	2	2	30	30	20	20	93	93
	12 × dorsal vertebrae	17	17	18	18	14	14	8	8	6	6	8	8	0	0	5	5	78	78	41	41	195	195
	5 × lumbar vertebrae	8	8	7	7	5	5	2	2	2	2	0	0	2	2	3	3	39	39	18	18	86	86
	Sacrum	4	4	3	3	2	2	0	0	0	0	0	0	1	1	1	1	4	6	4	4	19	21
	2 × iliac bones	11	24	8	12	4	6	2	4	1	2	2	4	1	2	2	4	10	22	8	16	49	96
	2 × pubic bones	3	3	3	3	0	0	0	0	0	0	1	2	1	1	0	0	3	6	2	4	13	19
	2 × femurs	12	22	8	11	5	7	2	3	1	2	0	0	1	2	1	2	8	16	8	10	46	75
	2 × tibias	5	9	6	8	2	4	0	0	0	0	2	4	0	0	0	0	4	6	4	8	23	39
	Total skeletal metastases	171	208	137	150	66	75	26	31	30	36	30	37	12	16	15	19	286	326	211	239	984	1137
Organs	Brain	2	3	1	2	0	0	0	0	0	0	0	0	0	0	0	0	4	6	2	2	9	13
	Lung	3	14	3	7	1	3	2	7	1	3	2	8	0	0	0	0	2	4	3	8	17	54
	Liver	4	12	1	3	3	11	3	13	0	0	0	0	0	0	0	0	2	5	3	8	16	52
	Others	0	0	0	0	0	0	0	0	0	0	0	0	0	0	0	0	4	6	8	12	12	18
	Total organ metastasis	9	29	5	12	4	14	5	20	1	3	2	8	0	0	0	0	12	21	16	30	54	137
Total		219	318	169	200	90	127	42	74	38	59	39	65	20	44	19	30	367	462	268	360	1271	1739

Abbreviations: *LN* lymph node, *R* total number of involved metastatic *regions* from a specific primary tumor, *L* total number of *lesions* detected in a specific region from a specific primary tumor, *HL* Hodgkin's lymphoma, *NHL* non-Hodgkin's lymphoma

Table 5 Sensitivities, specificities, and accuracies expressed per regions involved

		Positive		Negative		Sensitivity		Specificity		PPV		NPV		Accuracy	
		TP	FP	TN	FN	Value	95% CI	Value	95% CI	Value	95% CI	Value	95% CI	Value	95% CI
LNs (16 regions)	2 × Cervical	26	13	44	9	74	57–88	77	64–87	67	54–77	83	73–90	76	66–84
	Mediastinal	10	5	21	10	50	27–73	81	61–93	67	45–83	68	57–77	67	52–80
	2 × supra-clavicular	8	7	67	10	44	22–69	91	81–96	53	32–73	87	81–91	82	72–89
	2 × axillary	27	18	42	5	84	67–95	70	57–81	60	50–69	89	79–95	75	65–83
	Para-aortic	16	1	27	2	89	65–98	96	82–100	94	70–99	93	78–98	93	82–99
	Porta-hepatis	9	0	36	1	90	56–100	100	90–100	100		97	85–100	98	88–100
	Mesenteric	8	3	32	3	73	39–94	91	77–98	73	46–89	91	80–97	87	74–95
	2 × iliac	19	5	63	5	79	58–93	93	84–98	79	61–90	93	85–97	89	81–95
	2 × femoral	12	9	71	0	100	74–100	89	80–95	57	42–71	100		90	82–95
	2 × inguinal	19	18	54	1	95	75–100	75	63–84	51	41–61	98	89–100	79	70–87
	Total LNs	154	79	457	46	77	71–83	85	82–88	66	61–71	91	88–93	83	80–86
Skeletal system (63 regions)	Skull	11	1	32	2	85	55–98	97	84–100	92	61–99	94	82–98	93	82–99
	2 × clavicle	26	8	53	5	84	66–95	87	76–94	76	63–86	91	83–96	86	77–92
	Sternum	14	3	26	3	82	57–96	90	73–98	82	61–93	90	75–96	87	74–95
	2 × humerus	33	6	49	4	89	75–97	89	87–96	85	72–92	92	83–97	89	81–95
	24 × ribs	339	19	718	28	92	89–95	97	96–98	95	92–97	96	95–97	96	94–99
	7 × cervical vertebrae	76	17	210	19	80	71–88	93	88–96	82	74–88	92	88–94	89	85–92
	12 × dorsal vertebrae	176	19	334	23	88	83–93	95	92–99	90	86–94	94	91–96	92	90–94
	5 × lumbar vertebrae	70	16	133	11	86	77–93	89	83–94	81	73–88	92	87–95	88	83–92
	Sacrum	15	4	25	2	88	64–99	86	68–96	79	60–91	93	77–98	87	74–95
	2 × iliac bones	40	9	38	5	89	76–96	81	67–91	82	71–89	88	77–95	85	76–91
	2 × pubic bones	12	1	71	8	60	36–81	99	93–100	92	62–99	90	84–94	90	82–95
	2 × femurs	35	11	43	3	92	79–98	80	66–89	76	65–84	93	83–98	85	76–91
	2 × tibias	20	3	66	3	87	66–97	96	88–99	87	69–95	96	88–98	93	86–98
	Total skeletal metastases	867	117	1798	116	88	86–90	94	93–95	88	86–90	94	93–95	92	91–93
Organs	Brain	7	2	35	2	78	40–97	95	82–99	78	47–93	95	84–98	91	79–98
	Lung	14	3	21	8	64	41–83	88	68–97	82	61–93	72	60–82	76	61–87
	Liver	16	0	30	0	100	97–100	100	88–100	100		100		100	92–100
	Others	11	1	30	4	73	45–92	97	83–100	92	61–99	88	76–95	89	76–96
	Total organ metastasis	48	6	116	14	77	65–87	95	90–98	89	78–95	89	84–93	89	84–93
Total		1069	202	2371	176	86	84–88	92	91–93	84	82–86	93	92–94	90	89–91

Abbreviations: *LN* lymph node, *TP* true-positive, *FP* false-positive, *TN* true-negative, *FN* false-negative, *CI* confidence interval, *NPV* negative predictive value, *PPV* positive predictive value

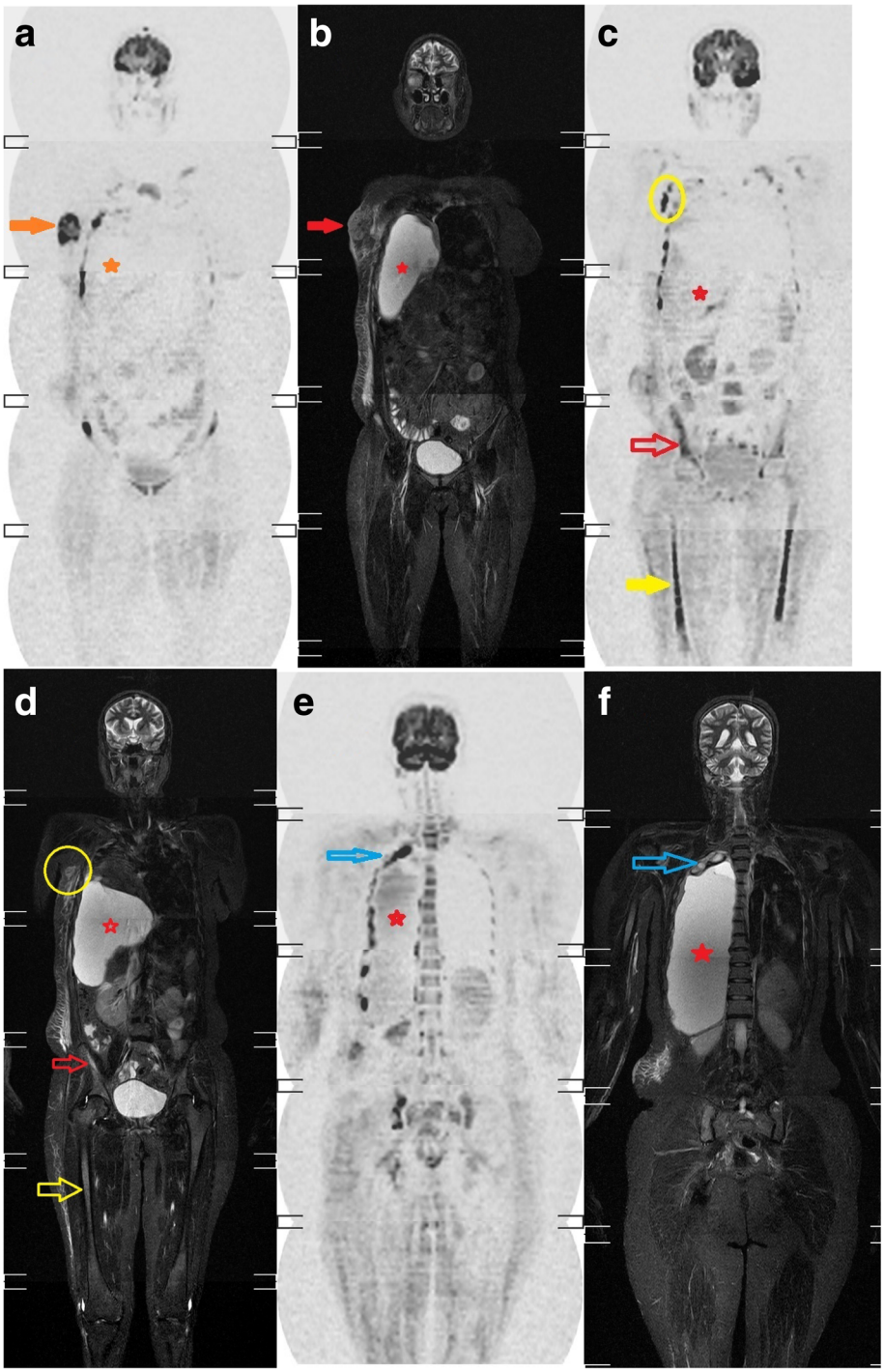

Fig. 1 A 54-year-old female patient diagnosed with metastatic breast cancer. **a** Inverted grey scale coronal WB-DWI and **b** coronal STIR show the primary right breast cancer (red arrows). **c** Inverted grey scale coronal WB-DWI and **d** coronal STIR show metastatic right axillary lymph nodes; the transverse diameter of one of them is 1.3 cm (yellow circle), metastasis of both femurs (yellow arrow) and right iliac bone (red arrow) shown as hyperintensity in STIR and restricted diffusion in DWI. **e** Inverted grey scale coronal WB-DWI and **f** coronal STIR show metastatic first right two ribs as well as multiple rib lesions (blue arrows). Marked right pleural effusion is noted in coronal STIR but does not show restricted diffusion in DWI (red stars)

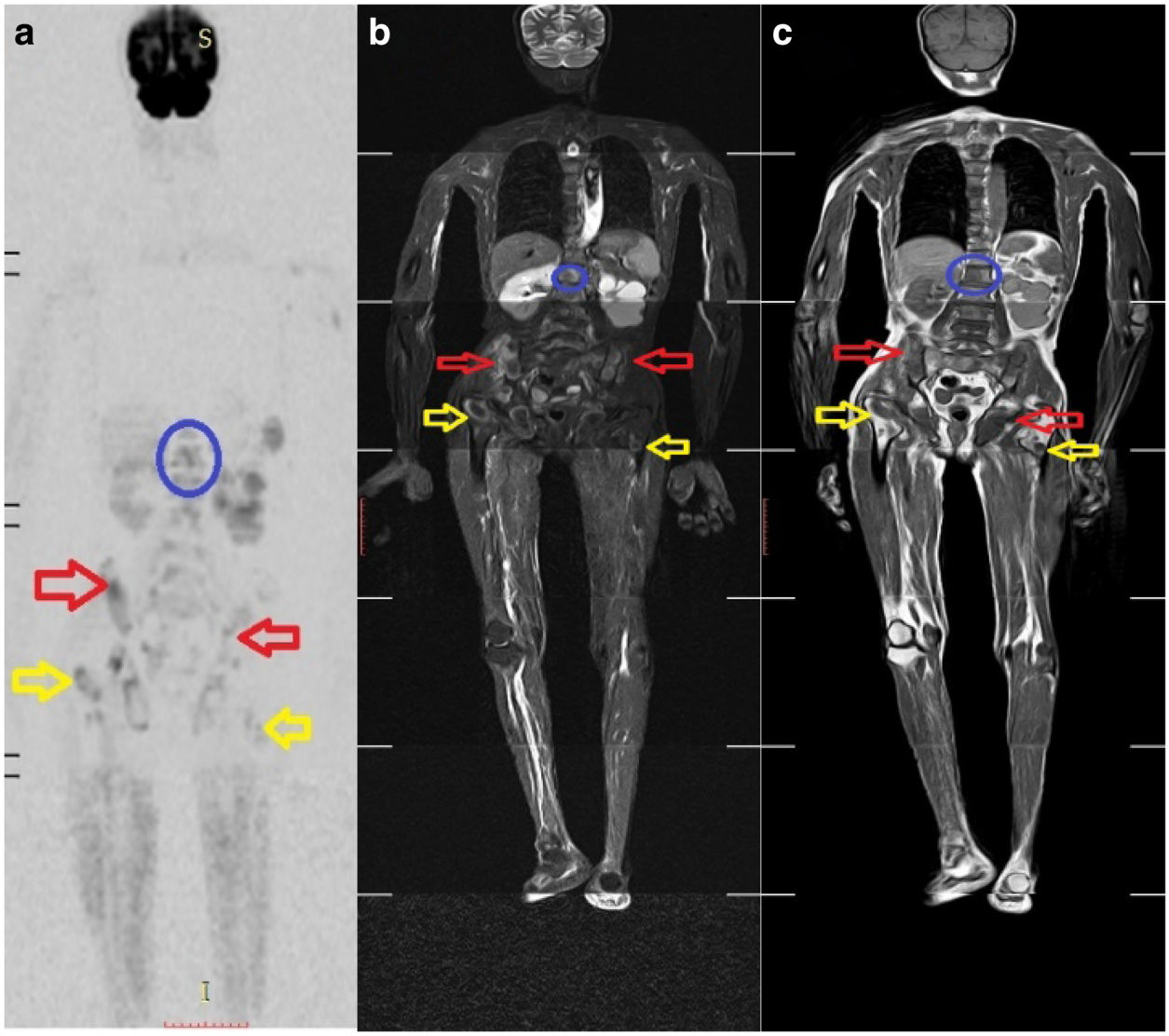

Fig. 2 A 62-year-old male patient with cancer prostate. Multiple bone metastases in vertebral bodies (blue circle), bilateral iliac bones (red arrows), and bilateral femoral heads (yellow arrows). **a** Inverted gray scale coronal WB DWI. **b** Coronal STIR. **c** Coronal T1 WI

them to each other, which does not happen in the clinical scenarios.

We did not restrict our inclusion to a specific disease or organ, either primary or secondary. Also, to get the highest yield from our limited research, we deliberately did not investigate the role of WB-MRI in assessment of tumor response.

In this study, to get the most accurate calculations, we divided the LN and skeletal groups to the smallest possible segments or regions. For example, ribs, we divided in 24 ribs; so every single rib is an independent region. Meanwhile, we did not divide organs into further smaller segments.

LN lesions

Regarding evaluating malignant metastatic or lymphomatous LNs, the relatively low sensitivity of WB-DWI-MRI in detection of regional nodal metastases in this study can be explained by the fact that metastases can be present in non-enlarged LN and not all enlarged nodes are malignant. Changing the size criteria towards larger or smaller cut-offs will influence sensitivity and specificity as a low threshold for cut-off values would increase the sensitivity, but specificity would decrease. This can explain the variation in the sensitivity of WB-DWI-MRI in other studies which ranges from 60 to 90% [4, 5]. The most accepted criterion for malignant LN

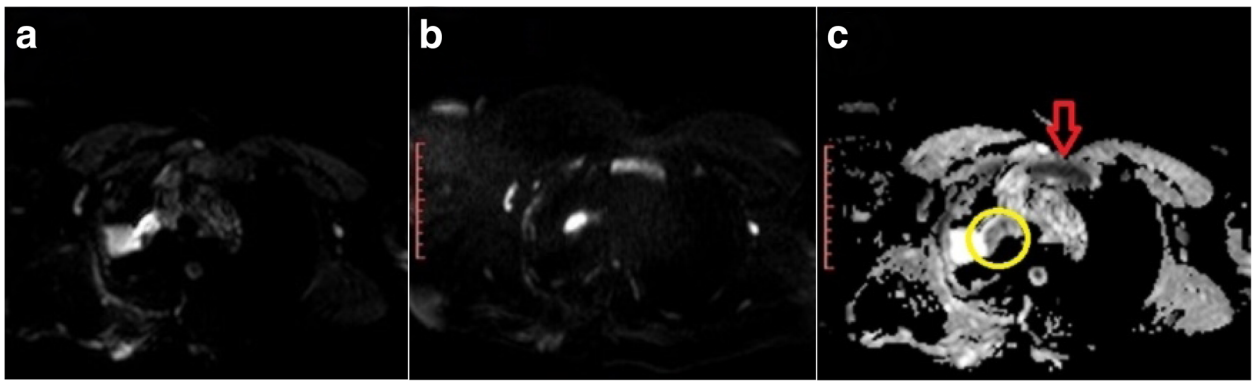

Fig. 3 A 45-year-old female patient with right apical lung cancer, epsilateral pleural effusion, and sternal metastasis. **a** Axial DWI. Medially located tumor and laterally located pleural effusion; both are showing restricted diffusion. **b** Axial DWI. Restricted diffusion of sternal metastasis. **c** ADC map. Low ADC in malignant tumor (yellow circle) and sternal metastasis (red arrow) but high in pleural effusion

involvement in conventional MRI sequences is that a short diameter greater than 8–10 mm [6]. A normal LN already has a relatively long T2 relaxation time and a restricted diffusion, due to their high cellularity, thus adding ADC values enhanced the discrimination between malignant and benign LNs. In this study, the combined usage of WB-DWI-MRI with the conventional sequences improved the detectability of LN metastasis. Seber et al. [7] in their study on differentiating benign from malignant LN infiltration from wide range of tumor types involving different body locations, found that adding DWI (utilizing an ADC cut-off value of 0.8×10^{-3} mm^2/s) to conventional MRI findings increased the accuracy from 80.6 to 91.6%.

There is a wide variability of accuracies within different sites in the study. The highest accuracy was found in porta-hepatis LNs. Whereas the lowest accuracy was found in mediastinal LNs where image quality may be affected by pulsation artifacts. The later finding was contrary to Sigovan et al.'s findings [8] where they showed high sensitivity, specificity, and accuracy (90.9%, 83%, and 85%, respectively) for DWI in differentiating benign from malignant enlarged mediastinal LNs.

One of the confusing pitfalls is splenic hilar lymphadenopathy with an accessory spleen, as both may be hyper-intense on STIR and DWI sequences. The same issue was reported by Massani et al. [9].

In our study, there were no differences in DWI values between Hodgkin disease and non-Hodgkin's lymphoma. Interestingly, Sabri et al. [10], in their study on malignant mediastinal LN involvement, detected a significant difference between the ADC values of Hodgkin disease and non-Hodgkin lymphoma.

Skeletal system lesions

In this study, WB-DWI-MRI identified 1137 bony lesions in 984 regions. The sensitivity, specificity, and accuracy were 88%, 94%, and 92%, respectively. Similar to other studies, we noted that the sole evaluation of bone lesions by DWI, STIR, or T2-WI makes high false-positive results of non-tumor lesions as in anemia, smoking, spondylodiscitis, osteomyelitis, bone infarctions, hemangiomas, and fractures which cause increased signal due to bone marrow edema [11–13]. The use of ADC maps and T1-WI in these occasions could decrease the false-positive results. Sagittal STIR of whole spine was included for evaluation of all the vertebrae to improve the accuracy of lesion localizations due to a higher spatial resolution [14]. False-negative results were found in the areas prone to motion artifacts as the sternum and clavicles. They were more obvious in conventional sequences than in WB-DWI [15, 16].

Brain lesions

WB-DWI-MRI only provide information about tumor cellularity, and this may explain its low sensitivity of 78% and high specificity 95% in this study as it could correctly identify 13 lesions of the brain in 9 patients. This was evident in other studies as well and is believed to be due to inherent high signal of the brain [17]. In suspected brain lesions, FLAIR sequence was exceptionally added to confirm the diagnosis, which is capable to elucidate areas of vasogenic edema around the tumor [18]. Ahmed and Mokhtar [19] reported similar finding to ours in their study on cerebral lesions. They found that there are mixed diffusion changes in most of the lesions in their study, and there was overlap in the measured ADC values between neoplastic and non-neoplastic lesions. On the other hand, Berghoff et al. [20] reported that ADC values correlated with survival and recurrence after surgical resection. Additionally, Lee et al. [21] reported that it correlated with survival after radiosurgery. Another interesting finding was reported

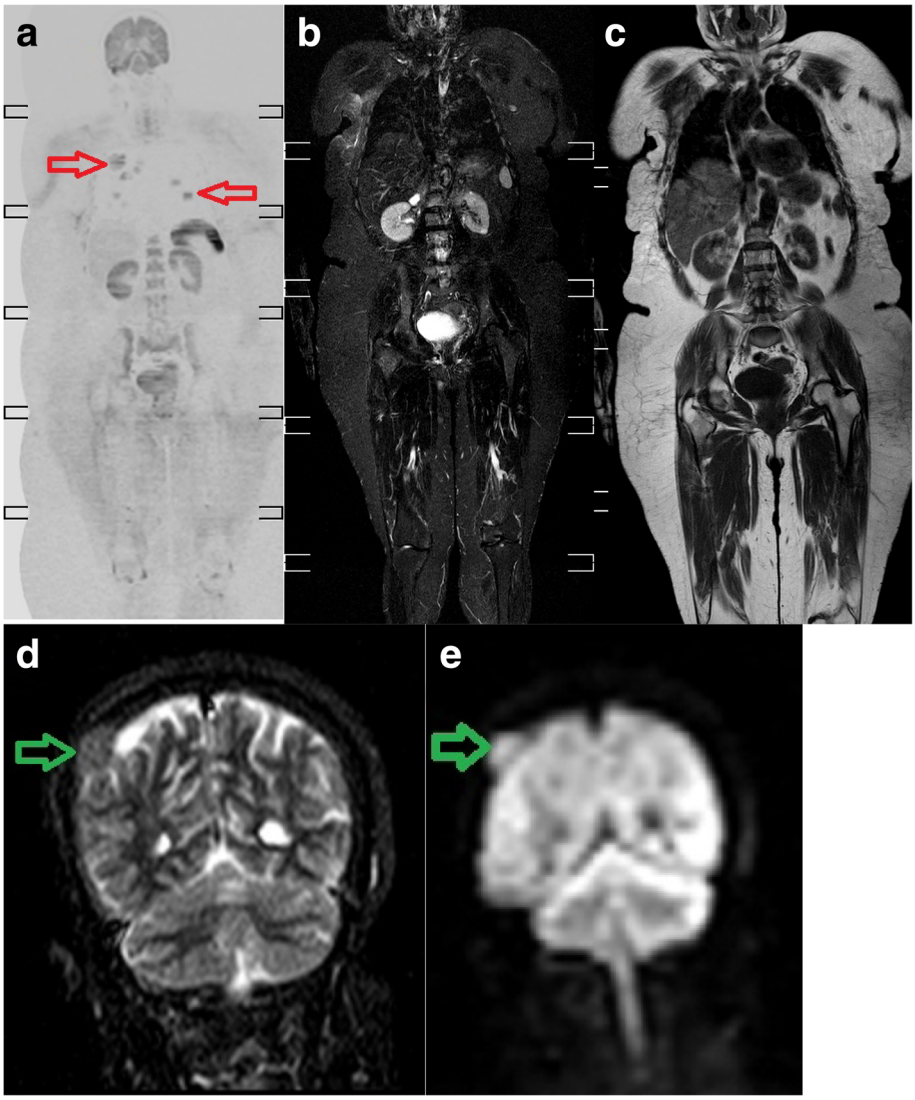

Fig. 4 A 61-year-old female patient, diagnosed with right breast cancer. Metastatic lesions were suspected. **a** Inverted grey scale coronal WB-DWI: multiple cannon ball metastatic lesions (red arrows) distributed bilaterally which are not seen in coronal STIR (**b**) or coronal T1 WI (**c**). Right parietal bone metastatic lesion (green arrows) seen as hyper intensity in coronal STIR (**d**) and restricted diffusion in coronal DWI (**e**)

by Zakaria et al. [22], that ADC changes at the tumor edge may indicate a more aggressive phenotype.

Pulmonary lesions

WB-MRI identified 54 lesions in 17 patients. Sensitivity, specificity, and accuracy were 64%, 88%, and 76%, respectively. This was lower than that of other conventional imaging as CT in many studies [23]. This can be attributed to difficulties in detection of small metastatic lung nodules (less than 8 mm). Free-breathing DWI acquisition in this study led to reduced accuracy of lesion detection (especially lung bases) due to respiratory movements and cardiac motion [23]. Also, lesions located at air-tissue interfaces were more difficult to be identified. Similarly, Regier et al. [24] reported sensitivity of 97% for nodules larger than 10 mm, but for 6–9 mm nodules, the sensitivity decreased to 86%, and for nodules 5 mm or smaller, it decreased to 43.8%. Similar finding was reported by Liu et al. [25] in assessing pulmonary metastases in patients with renal cell carcinoma. The use of ADC mapping added a value of discrimination between benign and malignant nodules [26]. A recent meta-analysis reported sensitivity and specificity of DWI to be 82.8% and 80.1%, respectively [27].

Liver lesions

Regarding hepatic metastases, WB-MRI had an accuracy of 100%. Thanks to the use of combined DWI with ADC together with anatomical localization by conventional MRI, the detection rate of malignant focal hepatic lesion

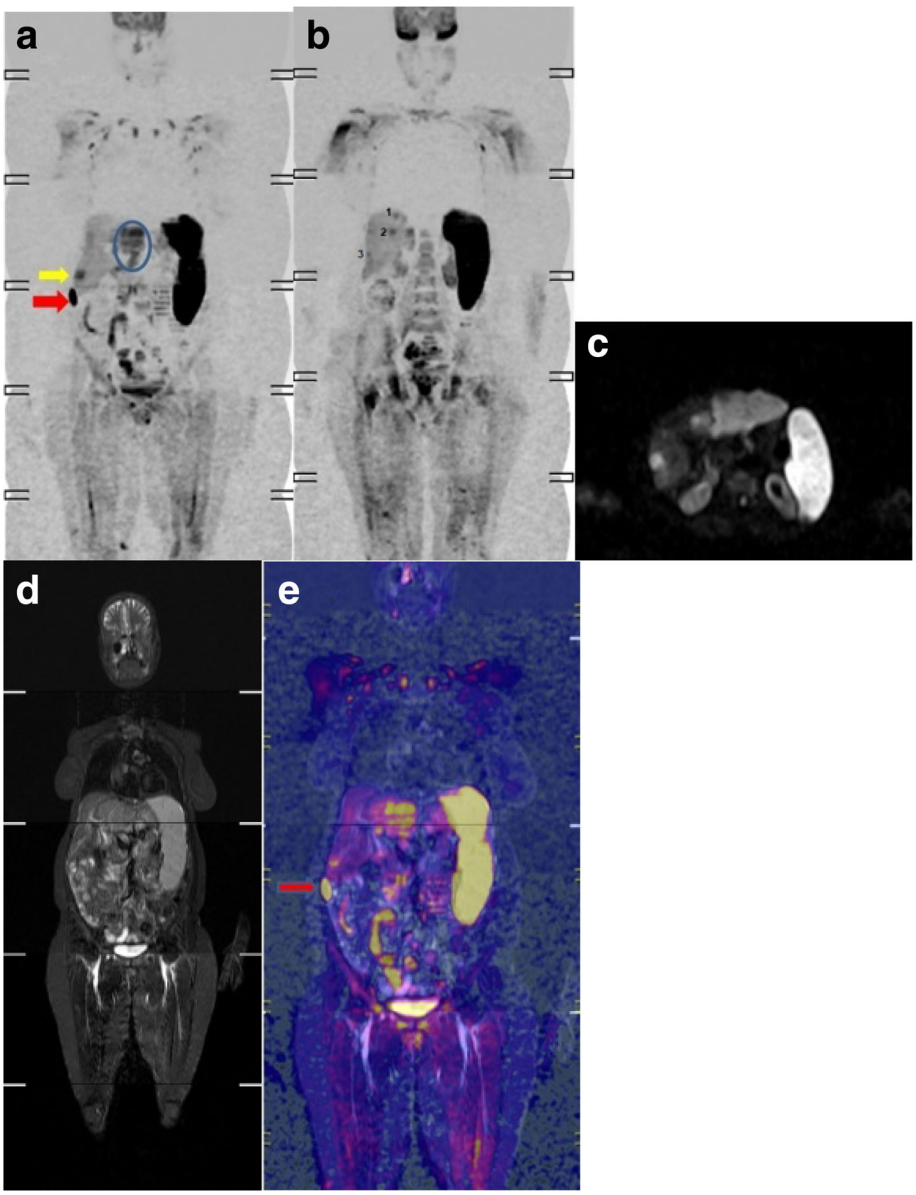

Fig. 5 A 55-year-old female patient with metastatic hepatocellular carcinoma (HCC). **a** Coronal WB DWI. Left lobe HCC (circle) and a metastatic hepatic focal lesion (yellow arrow). Note splenomegaly. **b** Coronal WB DWI. Multiple metastatic hepatic focal lesions (three lesions). **c** Axial DWI. Left lobe HCC and hepatic focal lesions. **d** Coronal STIR. Liver lesions are not clearly shown as in DWI. **e** Fusion images of both DWI and STIR. Hepatic flexure of the colon can be misinterpreted as a hepatic focal lesion (red arrow)

was high. These results were also reported in another study [28]. Another explanation to these high results in this study as whole organ is considered a single region. As there was usually more than one lesion in the liver, if only one of them was correctly detected, the researchers would consider this scan a true-positive; the others will not be reported. WB-MRI is comparable with contrast-enhanced CT or contrast-enhanced MRI but with advantage that it does not require contrast medium [29]. Of particular interest, Abou-Khadrah and Bedeer [30] in a prospective study showed that DWI is beneficial in small hepatocellular carcinomas smaller than 2 cm where they reported high sensitivity, specificity, and accuracy of combined conventional MRI and diffusion (92.8%, 71.4%, and 93.3%, respectively).

Study limitations

There are some limitations to the study. It included a heterogenous group of patients with different pathologies, so, each pathology was represented by a small number of patients. Our aim was to do an exploratory study for the value of WB-DWI-MRI in detecting metastases,

by including different types of malignancies and lymphomas in a single study. To minimize the effect of small study size, we deliberately did not investigate the role of WB-MRI in assessment of tumor response. Another limitation to the study is that histological examination to confirm the nature of the lesion was possible in only a small number of lesions. This study was conducted in clinical setting, and biopsies were requested by the treating physicians for the clinical requirements not for the sake of the study. This study was prospectively conducted and included only those patients who could be followed up by different radiological examinations for periods that were deemed sufficient to prove that a specific radiological finding is metastatic or not base upon its biological behavior.

Conclusion

The diagnostic performance of WB-DWI-MRI combined with conventional MRI and ADC mapping is variable among different anatomical sites. It has good performance in diagnosis of some organs as liver, bone marrow, and some LNs as porta-hepatis. It has a less diagnostic performance in the lung, and LNs located in cervical, mediastinum, supraclavicular, and mesenteric regions.

Abbreviations

ADC: Apparent diffusion coefficient; FLAIR: Fluid-attenuated inversion recovery; LN: Lymph node; PET/CT: Positron emission/computed tomography; T1-WI, T2-WI: T1- or T2-weighted images; WB-DWI-MRI: Whole-body diffusion-weighted magnetic resonance imaging

Acknowledgements

Not applicable.

Authors' contributions

AA, EA, HIM, and HGM conceived and designed the analysis. MK and HG collected the data. AT and HG performed the analysis, and HG wrote the manuscript. All authors read and approved the final manuscript.

Funding

This research received no specific grant from any funding agency in the public, commercial, or not-for-profit sectors.

Availability of data and materials

The datasets used and/or analyzed during the current study are available from the corresponding author on reasonable request.

Ethics approval and consent to participate

Ethics approval was obtained by Faculty of Medicine Ethical Committee, Assiut University, Egypt. Ethical approval was obtained in the meeting held by the committee on 11-05-2014. No reference number was issued by the committee. Signed committee approval is kept by the researchers. Written patients' informed consents for participation in this study were taken and kept.

Consent for publication

All patients included in this research gave written informed consent to publish the data contained within this study.

Competing interests

The authors declare that they have no competing interests.

Author details

[1]Radiology Department, Faculty of Medicine, Assiut University, Assiut, Egypt. [2]Medical Oncology Department, Faculty of Medicine, Assiut University, Assiut, Egypt. [3]Surgery Department, Faculty of Medicine, Assiut University, Assiut, Egypt.

Received: 17 April 2020 Accepted: 23 June 2020
Published online: 29 July 2020

References

1. Heindel W, Gubitz R, Vieth V, Weckesser M, Schober O, Schafers M (2014) The diagnostic imaging of bone metastases. Dtsch Arztebl Int 111(44):741–747
2. Kwee TC, van Ufford HM, Beek FJ, Takahara T, Uiterwaal CS, Bierings MB et al (2009) Whole-body MRI, including diffusion-weighted imaging, for the initial staging of malignant lymphoma: comparison to computed tomography. Invest Radiol 44(10):683–690
3. Pasoglou V, Michoux N, Larbi A, Van Nieuwenhove S, Lecouvet F (2018) Whole Body MRI and oncology: recent major advances. Br J Radiol 91(1090): 20170664
4. Albano D, Patti C, La Grutta L, Agnello F, Grassedonio E, Mule A et al (2016) Comparison between whole-body MRI with diffusion-weighted imaging and PET/CT in staging newly diagnosed FDG-avid lymphomas. Eur J Radiol 85(2):313–318
5. Balbo-Mussetto A, Cirillo S, Bruna R (2016) Whole-body MRI with diffusion-weighted imaging: a valuable alternative to contrast-enhanced CT for initial staging of aggressive lymphoma. Clin Radiol 71(3):271–279
6. de Bondt RBJ, Nelemans PJ, Bakers F, Casselman JW, Peutz-Kootstra C, Kremer B et al (2009) Morphological MRI criteria improve the detection of lymph node metastases in head and neck squamous cell carcinoma: multivariate logistic regression analysis of MRI features of cervical lymph nodes. Eur Radiol 19(3):626–633
7. Seber T, Caglar E, Uylar T, Karaman N, Aktas E, Aribas BK (2015) Diagnostic value of diffusion-weighted magnetic resonance imaging: differentiation of benign and malignant lymph nodes in different regions of the body. Clin Imaging 39(5):856–862
8. Sigovan M, Akl P, Mesmann C, Tronc F, Si-Mohamed S, Douek P et al (2018) Benign and malignant enlarged chest nodes staging by diffusion weighted MRI: an alternative to mediastinoscopy? Br J Radiol 91(1082):20160919
9. Massani M, Maccatrozzo P, Morana G, Fabris L, Ruffolo C, Bonariol L et al (2016) Diagnostic difficulties and therapeutic choices in intrapancreatic accessory spleen: case reports. Open Access Surgery 9:15–20
10. Sabri YY, Nossair EZB, Assal HH (2020) Role of diffusion weighted MR-imaging in the evaluation of malignant mediastinal lesions. Egypt J Radiol Nucl Med 51:32
11. Jambor I, Kuisma A, Ramadan S (2016) Prospective evaluation of planar bone scintigraphy, SPECT, SPECT/CT, 18F-NaF PET/CT and whole body 1.5 T MRI, including DWI, for the detection of bone metastases in high risk breast and prostate cancer patients: SKELETA clinical trial. Acta Oncol 55(1):59–67
12. Lecouvet FE, El Mouedden J, Collette L (2012) Can whole-body magnetic resonance imaging with diffusion-weighted imaging replace Tc 99m bone scanning and computed tomography for single-step detection of metastases in patients with high-risk prostate cancer? Eur Urol 62(1):68–75
13. Balliu E, Boada M, Peláez I (2010) Comparative study of whole-body MRI and bone scintigraphy for the detection of bone metastases. Clin Radiol 65(12): 989–996
14. Stecco A, Trisoglio A, Soligo E, Berardo S, Sukhovei L, Carriero A (2018) Whole-Body MRI with Diffusion-Weighted Imaging in Bone Metastases: A Narrative Review. Diagnostics (Basel) 8(3):45
15. Koh D-M, Blackledge M, Padhani AR, Takahara T, Kwee TC, Leach MO et al (2012) Whole-Body Diffusion-Weighted MRI: Tips, Tricks, and Pitfalls. Am J Roentgenol 199(2):252–262
16. Padhani AR, Koh DM, Collins DJ (2011) Whole-body diffusion-weighted MR imaging in cancer: current status and research directions. Radiology 261(3): 700–718
17. Duygulu G, Ovali GY, Calli C, Kitis O, Yunten N, Akalin T et al (2010) Intracerebral metastasis showing restricted diffusion: correlation with histopathologic findings. Eur J Radiol 74(1):117–120
18. Mehrabian H, Detsky J, Soliman H, Sahgal A, Stanisz GJ (2019) Advanced magnetic resonance imaging techniques in management of brain metastases. Front Oncol 9:440
19. Ahmed HAK, Mokhtar H (2020) The diagnostic value of MR spectroscopy versus DWI-MRI in therapeutic planning of suspicious multi-centric cerebral lesions. Egyptian Journal of Radiology and Nuclear Medicine 51(1)

20. Berghoff AS, Spanberger T, Ilhan-Mutlu A, Magerle M, Hutterer M, Woehrer A et al (2013) Preoperative diffusion-weighted imaging of single brain metastases correlates with patient survival times. PLoS One 8(2):e55464
21. Lee CC, Wintermark M, Xu Z, Yen CP, Schlesinger D, Sheehan JP (2014) Application of diffusion-weighted magnetic resonance imaging to predict the intracranial metastatic tumor response to gamma knife radiosurgery. J Neuro-Oncol 118:351–361
22. Zakaria R, Das K, Radon M, Bhojak M, Rudland PR, Sluming V et al (2014) Diffusion-weighted MRI characteristics of the cerebral metastasis to brain boundary predicts patient outcomes. BMC Med Imaging 14:26
23. Paruthikunnan SM, Kadavigere R, Karegowda LH (2017) Accuracy of whole-body DWI for metastases screening in a diverse group of malignancies: comparison with conventional cross-sectional imaging and nuclear scintigraphy. Am J Roentgenol 209(3):477–490
24. Regier M, Schwarz D, Henes FO (2011) Diffusion-weighted MR-imaging for the detection of pulmonary nodules at 1.5 Tesla: intraindividual comparison with multidetector computed tomography. J Med Imaging Radiat Oncol 55(3):266–274
25. Liu J, Yang X, Li F, Wang X, Jiang X (2011) Preliminary study of whole-body diffusion-weighted imaging in detecting pulmonary metastatic lesions from clear cell renal cell carcinoma: comparison with CT. Acta Radiol 52(9):954–963
26. Tang J, Leung B, Lee D, Sung H, Cheng C (2019) Multimodality imaging spectrum of extranodal lymphoma: a pictorial review. Hong Kong J Radiol 22:67–77
27. Li B, Li Q, Chen C, Guan Y, Liu S (2014) A systematic review and meta-analysis of the accuracy of diffusion-weighted MRI in the detection of malignant pulmonary nodules and masses. Acad Radiol 21(1):21–29
28. Shenoy-Bhangle A, Baliyan V, Kordbacheh H, Guimaraes AR, Kambadakone A (2017) Diffusion weighted magnetic resonance imaging of liver: principles, clinical applications and recent updates. World J Hepatol 9(26):1081–1091
29. Riviere DM, van Geenen EJM, van der Kolk BM, Nagtegaal ID, Radema SA, van Laarhoven C et al (2019) Improving preoperative detection of synchronous liver metastases in pancreatic cancer with combined contrast-enhanced and diffusion-weighted MRI. Abdom Radiol (NY) 44(5):1756–1765
30. Abou khadrah RS, Bedeer A (2019) A small hepatic nodule (≤ 2 cm) in cirrhotic liver: doTriphasic MRI and Diffusion-weighted image help in diagnosis. Egyptian Journal of Radiology and Nuclear Medicine 50(1).

Publisher's Note